

duction, gaming and AR/VR. 3D generation models have witnessed remarkable progress which can be attributed to the scalability of 3d generative models [24, 35, 39, 43], and utilization of the large-scale training datasets [10]. However, most existing 3D mesh and texture generation models often lack PBR material properties so they lose the view-dependent photorealistic effect. Furthermore, the textures, which incorporate pre-baked shadows and lighting, restrict their applicability in downstream tasks.

PBR estimation from images is a recent development in the field of 3D assets with PBR generation, such as Clay [49] has demonstrated impressive capabilities in 3D mesh with PBR materials generation, but they rely on expensive geometric prior to ensure cross-view PBR consistency. 3DTopia-XL [8] encodes detailed shape, Albedo, and material field into a Diffusion Transformer (DiT) framework. To achieve better performance, these methods have attempted to incorporate BSDF and illumination models into 3D generation model. More recently, Meta3DAssetGen [37] exploit to integrate the differentiable BRDF optimization model into forward transformer-based architecture. SF3D [2] incorporates explicit lighting and a differentiable shading model for decomposing light from UV texture.

In the field of 3D generation, PBR material representation has recently emerged as a key advancement, significantly improving the rendering quality of generated objects. For example, Clay [49] has demonstrated impressive capabilities to generate PBR materials for 3D meshes, yet it requires geometric input to maintain cross-view consistency and concurrently suffers from the deterioration of detailed textures. 3DTopia-XL [8] develops a primitive presentation to encode detailed shape, Albedo, and material fields into a Diffusion Transformer (DiT) framework. On the other hand, recent methods have attempted to incorporate BSDF material functions and illumination models into 3D generation models. Meta3DAssetGen [37] exploits the integration of the differentiable BRDF optimization model into a large reconstruction model (LRM) with a forward transformer-based architecture. SF3D [2] incorporates explicit lighting and a differentiable shading model for decomposing light from UV textures.

However, by simplifying material models with a single illumination for different objects and ignoring the spatially varying properties of metalness and roughness, these methods face three significant limitations that hinder their widespread adoption. Firstly, these methods are more likely to bake high light into the Albedo map due to the existing ambiguity between illumination and Albedo, especially for reflective objects. Secondly, roughness and metallicity are difficult to observe directly from RGB images. We also noticed that the BRDF distribution in current synthetic 3D datasets, such as Objaverse [10], exhibits a strong long-tail effect. This causes models to overfit to frequent values while

ignoring rare ones. As a result, the quality of PBR material generation is compromised, and spatially-varying attributes are poorly represented. Additionally, Meta3DAssetGen [37] employs LRM to predict PBR materials, which is trained from scratch. Given the scarcity of high-quality 3D PBR data, the generalization capability of the LRM may not be as strong as that of diffusion models for predicting PBR. Meanwhile, the performance of sparse-view reconstruction models can decline if the quality of multiple views is poor, as these models generally depend exclusively on view-aware RGB images to predict 3D representations.

In response to these challenges, we propose an efficient approach for high-quality 3D mesh with PBR materials generation from a single image or text prompt that disentangles the highlight and reconstructs spatially-varying metallic and roughness to enable relighting (see Fig.1). Our method introduces PBR3DGen, a two-stage 3D mesh generation method with high-fidelity PBR materials that integrates the novel PBR multiview diffusion models and PBR-based sparse-view reconstruction models to achieve high-quality 3D mesh with PBR materials generation. In the first stage, we leverage vision language models (VLM) like GPT-4V and view-dependent illumination-aware conditions to guide our multi-view PBR estimation model. Specifically, we employ VLM to precisely capture the spatial distribution and inherent attributes of reflective-metallic materials. This detailed information is then seamlessly integrated into a PBR multi-view diffusion model. This integration plays a pivotal role in drastically mitigating the ambiguity often encountered between specular highlights and Albedo within the rendered imagery. Furthermore, it addresses the issue of prediction inaccuracies in metallic and roughness properties, which were previously exacerbated by the severe long-tail distribution of training data. Consequently, our approach significantly enhances the consistency of part-aware material representation. In addition, we inject view-dependent illumination-aware conditions to enhance the spatially varying material properties. In the second stage, unlike most sparse-view reconstruction models that reconstruct 3D assets using only rgb color, we propose our PBR-based large reconstruction model, which employs a dual-head VAE encoder to separately encode the Albedo and Metallic-Roughness maps. Subsequently, we reconstruct the 3D mesh and PBR materials from the input PBR multi-view images.

In summary, our key contributions to the field of PBR 3D reconstruction are as follows:

- We propose PBR3DGen, a novel two-stage generation framework for 3D assets with high-quality PBR materials from image or text inputs;
- We explore leveraging vision-language models to guide PBR estimation within a multi-view diffusion model, enabling more accurate estimation of PBR materials and significantly reducing ambiguities between Albedo and

illumination, especially specular highlights.

- We introduce a view-dependent illumination-aware condition as a local pixel-wise prior, resulting in a more accurate capture of spatially varying reflectance effects.
- Our method exhibits superior 3D mesh and PBR material generation quality compared to current methods.

2. Related Works

2.1. Multi-view Diffusion

Cross-view consistency is crucial in a reconstruction-based 3D generation. MVDiffusion[39] first generates consistent multi-view images from text prompts, given pixel-to-pixel correspondences. SyncDreamer[22], MVDream[36], and Wonder3D[24] leverage attention mechanisms to facilitate information transfer between multi-view images, enhancing multi-view consistency. Zero123++[35] stitches multi-view images together while denoising them simultaneously, improving geometric consistency and texture quality. Era3D[19] introduces row-wise multi-view attention, reducing the computational overhead of multi-view generation. Although the quality of current multi-view image generation has made significant progress, multi-view images embed lighting and lack physical properties. In contrast to these previous methods, our approach not only maintains multi-view consistency but also provides PBR estimation. This enables our reconstruction results to support relighting and physically-based rendering.

2.2. Multi-view 3D Reconstruction

3D reconstruction has been a well-researched area in the field of computer vision for a long time. Although traditional methods such as Structure from Motion (SfM)[1, 26, 31] and Multi-View Stereo (MVS)[14, 27, 32] can perform camera calibration and 3D reconstruction, they lack robustness when dealing with inconsistent multi-view images. Recently, deep learning-based 3D reconstruction methods have become mainstream. LRM[16] first proposed utilizing a transformer backbone to simultaneously reconstruct geometry and texture through a single forward pass. LRM can learn how to reconstruct 3D geometry and texture from a single image using large-scale 3D datasets. Instant3D[20] increases the number of input views, further enhancing the geometric detail and texture quality of the reconstruction. Subsequent works[21, 42, 43, 47, 48] have made further improvements in reconstruction quality and computational efficiency. Compared to existing large reconstruction models, we not only reconstruct the 3D geometry, but we also reconstruct physics-based material properties, making the 3D assets generated by our method more realistic.

2.3. Diffusion-based PBR Material Generation

Material generation and estimation from RGB images is inherently difficult because of its under-constrained nature, including the ambiguity between illumination and materials. Diffusion models reveal the impressive capability of learning the distribution of the target domain, which has become prominent in texture content generation. Recent studies such as TEXTure [29], Text2Tex [5], TexFusion [4] extend the diffusion model to texture synthesis from multi-view images. SyncMVD [23] improves the consistency of multi-view texture by sharing the denoised content among different views in each denoising step to ensure texture consistency and avoid seams and fragmentation. However, these methods tend to generate RGB textures with highlights and shadows due to suffering from disentangling the materials and illumination properties. Recently, Paint3D [45] proposed a coarse-to-fine strategy to delight the generated texture in UV space, but they still lack Physically-based materials when dealing with inconsistent multi-view images. Fantasia3D [6] can generate more realistic textures by incorporating physics-based materials. FlashTex [11] introduces the lighting condition in ControlNet and optimizes texture based on Score Distillation Sampling loss, which can disentangle lighting from surface material/reflectance. However, these optimization-based methods require extensive training time. RGBX [46] utilizes diffusion models to estimate the Physically-based intrinsics of RGB images and demonstrates a significant improvement on the generalization. Additionally, IntrinsicAnything [7] only utilizes diffusion models to estimate albedo and specular shading from a single RGB image, which lacks roughness and metallic properties in 2D diffusion prior stage. Meanwhile, these methods still suffer from disentangling the spatially varying materials from highlight and reflective object images.

3. Methods

3.1. Overview

In this section, we introduce our high-quality 3D mesh with PBR materials generation pipeline, illustrated in Fig.2. Firstly, we establish a novel multi-view PBR texture diffusion model from a single image or text prompt, which unleashes Vision Language model (VLM) and illumination-aware conditions to guide PBR material generation. Secondly, we further design dual-head reconstruction model by extending a sparse-view large reconstruction model to handle multi-view PBR material inputs, significantly boosting the 3D mesh and texture reconstruction quality.

3.2. Multi-view PBR Estimation

Without prior geometric information, generating multi-view PBR materials directly from a single RGB image using a diffusion model is a challenging problem. Due to the in-

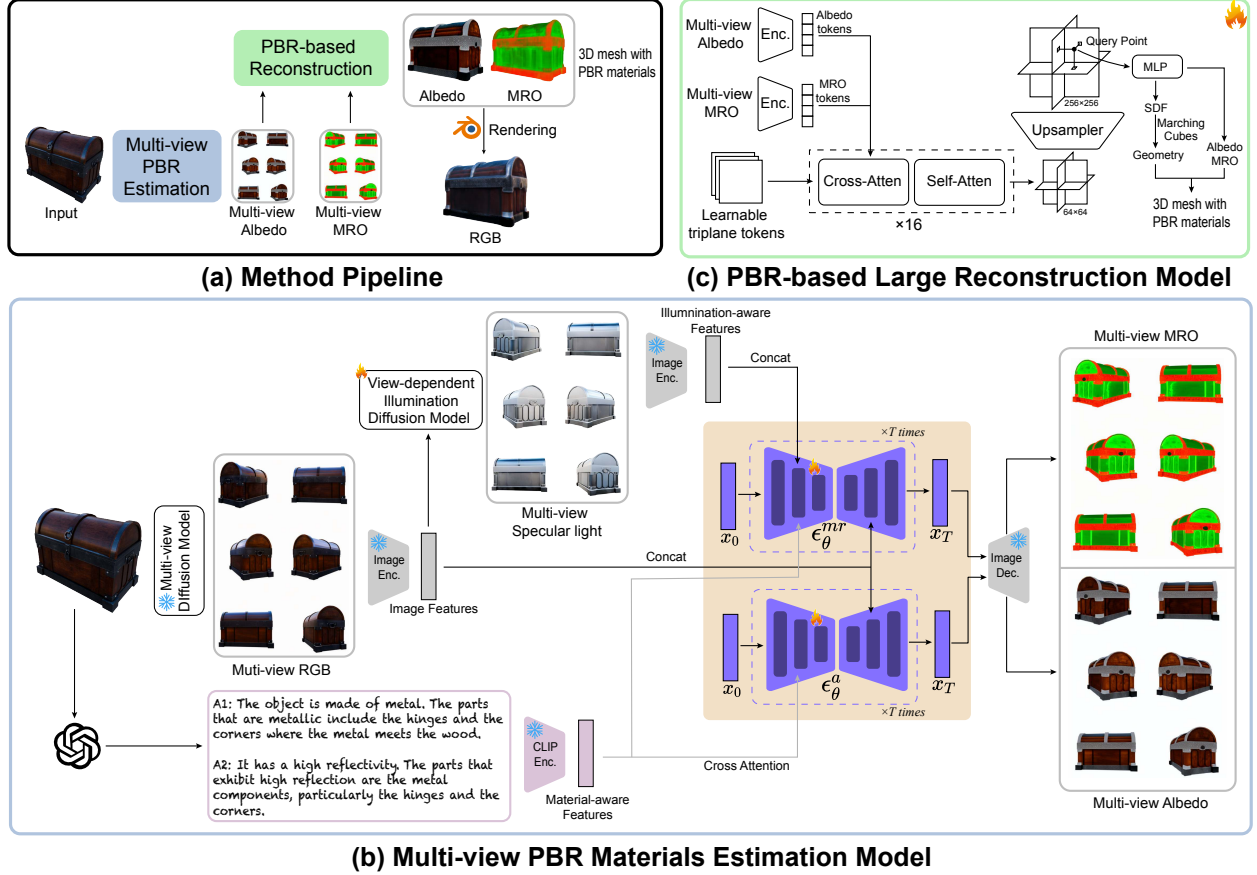


Figure 2. Method overview. Our method consists of two stages: Multi-view PBR materials estimation and 3D mesh with PBR materials reconstruction. Given an RGB image as input, we first generate multi-view Albedo images and multi-view MRO images using Multi-view PBR estimation model, and then reconstruct 3D assets with Dual-head PBR-based large reconstruction model.

herent ambiguities between material properties and lighting conditions, and the observation that the local distribution of material characteristics does not always align with geometric consistency. Multi-view PBR estimation from an RGB image cannot achieve both high-quality PBR materials and geometrically consistent multi-view images simultaneously. Therefore, We first resolve multi-view consistency by applying an off-the-shelf Multi-view Diffusion Model, such as Zero123++[35]. Meanwhile, we propose a PBR generation module from the multi-view RGB image input by introducing VLM guidance and view-dependent illumination-aware condition, which can significantly handle the ambiguity between PBR and illumination well.

Multi-view PBR Material Estimation with SD. Since PBR material estimation can be seen as domain transfer from an RGB image, The diffusion model can be utilized to transfer from the RGB domain distribution to the PBR domain distribution. And we observed that Roughness and Metallic often interact to produce specular reflection effects on objects. In our methods, we combined two maps into a single MRO (Metallic/Roughness/Zero channel) for generation. Therefore, we can model the conditional distribution of

corresponding Albedo and Metallic-Roughness by utilizing the RGB image as the conditioning signal, as in IntrinsicAnything [7] and RGBX [46]. Specifically, we first use the pre-trained VAE image encoder \mathcal{E} to extract the conditional signal feature from input grid image I . Then, the diffusion process adds noise to the encoded latent $z = \mathcal{E}(x)$ producing a noisy latent z_t where the noise level increases over timesteps $x \in T$. We learn network ϵ_θ that predicts the noise added to the noisy latent z_t given image conditioning $\mathcal{E}(I)$. We minimize the following loss:

$$L = \mathbb{E}_{\mathcal{E}(x), \mathcal{E}(I), \epsilon, t} [\|\epsilon - \epsilon_\theta(z_t, t, \mathcal{E}(I))\|_2^2] \quad (1)$$

where z_t is the noisy latent feature of the input z with t uniformly sampled from $\{1, \dots, T\}$, and estimating ϵ from a Gaussian distribution, denotes $\epsilon \sim \mathcal{N}(0, 1)$. Here, we separately optimize double U-Net Network ϵ_θ^a and ϵ_θ^{mr} corresponding Albedo estimation and MRO estimation.

3.2.1. VLM-guided PBR Material generation

We observed that the Roughness and Metallic distributions for objects tend to be strongly part-aware consistent, and there are significant ambiguities between Albedo and specular light during the Albedo generation process, especially

for specular and metallic objects. This is due to the high variance in the diffusion inference procedure.

As argued above, the PBR material generation model requires a strong prior to alleviate these challenging ambiguities. Inspired by [13], VLM can recognize object materials and types due to its extensive prior knowledge of objects. We design a hierarchical VLM-guided material policy to obtain reflective-metallic material attributes through unleashing GPT-4V with a strong material knowledge, which helps us capture the reflective-metallic properties for the input RGB image. Specifically, we first gather global information about metallic and reflective properties, and then we further investigate which parts exhibit these relevant attributes. The pipeline of the designed hierarchical strategy is depicted in Fig.2(b), with detail provided in the Fig.11 of Appendix .

To effectively utilize reflective-metallic material information in the PBR diffusion model process, we inject material caption features into the U-Net. Specifically, we first use the CLIP text encoder [28] to extract language features from the material captions. Then, to inject the conditioning signal into the Albedo U-Net network ϵ_θ and the Metallic-Roughness U-Net network ϵ_σ , we capture the embedding relationship using cross-attention mechanism between the material caption language features and the noised latent of the U-Net. We reparameterize the loss functions of ϵ_θ^a and ϵ_θ^{mr} following the corresponding conditioning signals in Eq.2 and Eq.3:

$$L = \mathbb{E}_{\mathcal{E}(x), \mathcal{E}(I), \epsilon, t} [\|\epsilon - \epsilon_\theta^{mr}(z_t^{mr}, t, f_s(\mathcal{E}(I)), C_T(I))\|_2^2] \quad (2)$$

$$L = \mathbb{E}_{\mathcal{E}(x), \mathcal{E}(I), \epsilon, t} [\|\epsilon - \epsilon_\theta^a(z_t^a, t, C_T(I))\|_2^2] \quad (3)$$

where C_T denotes CLIP text feature encoder, z_t^a is the latent feature encoded from the ground truth Albedo at timestep t .

3.2.2. View-dependent illumination-aware condition

Although the designed VLM-guided material diffusion model can effectively handle part-wise properties by injecting material description information, Metallic-Roughness estimation still struggles to capture spatially varying properties, due to the challenges posed by the severe long-tail distribution effect in the training data. Therefore, it is essential to introduce additional physics-based prior information.

Physically Based Rendering (PBR) materials often utilize the spatially-varying bi-directional reflectance distribution functions (svBRDFs) to approximate the surface reflectance property with a set of decomposed intrinsic terms, which can encapsulate the interaction of light with the object surface. Following the popular specular svBRDFs model, like the Cook-Torrance model [9], we can observe that the Roughness and Metallic properties are closely integrated with the specular shading term. The detailed rendering equation is provided in the Appendix (Sec.A.1). Specifically, the render-

ing equation is rewritten as Eq. 4:

$$L_o(\hat{\mathbf{x}}, \omega_o) = L_{diff}(\hat{\mathbf{x}}, k_d, L_i) + L_{spec}(\hat{\mathbf{x}}, \omega_o, F_0(k_m), k_r, L_i) \quad (4)$$

where the rendering results comprise diffuse shading L_{diff} and specular shading L_{spec} , k_d and k_r represent Albedo and Roughness, k_m is metallic term related to the Fresnel term.

Previous methods [2, 37, 49] for generating Roughness and Metallic maps tend to homogenize the distribution of BRDF in synthetic 3D data. For example, in the widely used Objaverse dataset [10], we observe that the Metalness and Roughness of objects often have fixed values. This results in a lack of spatial variability in the BRDF distribution obtained through diffusion model training, which negatively impacts the accuracy of the Metalness and Roughness attributes. To overcome the severe impact of the long-tail distribution, and motivated by Eq.4, we propose introducing view-dependent illumination as a condition to guide the sampling process of Roughness and Metallic. We further reformulate the loss function shown in Eq.1 into the following form in Eq. 5:

$$L = \mathbb{E}_{\mathcal{E}(x), \mathcal{E}(I), \epsilon, t} [\|\epsilon - \epsilon_\theta(z_t^{mr}, t, f_s(\mathcal{E}(I)))\|_2^2] \quad (5)$$

where z_t^{mr} is the latent feature encoded from the ground truth Metallic-Roughness gt at time step t , f_s is a specular illumination diffusion model to generate spatially-varying illumination based on single RGB grid image I . This specular illumination map acts as a local cue, enhancing the Metallic and Roughness spatial distribution closely linked to the actual distribution of the object.

3.3. Dual-head PBR Reconstruction Model

Our PBR reconstruction model takes multi-view Albedo multi-view images and MRO images as input, and it outputs 3D assets with PBR material. Since our reconstruction model has two types of inputs, using a single image encoder to extract features from both types would cause the model to be unable to distinguish between them. Therefore, we use dual-head PBR encoders: one encoder is for encoding the Albedo images, and the other encoder is for encoding the MRO images. Then two kinds of image tokens and learnable triplane tokens are passed through a transformer backbone, outputting a low-resolution triplane. The low-resolution triplane has a resolution of 64 with 1024 channels. We use an upsampler similar to [44] to upsample the low-resolution triplane, ultimately obtaining a high-resolution triplane with a resolution of 256 and 120 channels. For each query point, we project it onto a triplane to get its triplane feature, and we use an MLP to predict its signed distance, Albedo and MRO.

Since NeRF[25] and 3D Gaussian[17] have difficulty generating high-quality meshes, and the training of DMTet[33] and Flexicubes[34] is unstable, we adopt NeuS[41] as our

3D representation and obtain the geometry through marching cubes. With geometry, Albedo, and MRO, we obtain 3D asset with PBR as our final output. During training, we apply image loss for both Albedo images and MRO images:

$$\begin{aligned}
L = & \sum_i \|I_{i,A} - I_{i,A}^{gt}\|_2^2 \\
& + \sum_i \|I_{i,MRO} - I_{i,MRO}^{gt}\|_2^2 \\
& + \lambda_{lips} \sum_i L_{lips}(I_{i,A}, I_{i,A}^{gt}) \\
& + \lambda_{lips} \sum_i L_{lips}(I_{i,MRO}, I_{i,MRO}^{gt}) \\
& + \lambda_{mask} \sum_i \|M_i - M_i^{gt}\|_2^2
\end{aligned} \tag{6}$$

where $I_{i,A}$, $I_{i,MRO}$, M_i , $I_{i,A}^{gt}$, $I_{i,MRO}^{gt}$ and M_i^{gt} denote rendered Albedo images, rendered MRO images, rendered mask images, ground truth Albedo images, ground truth MRO images, ground truth mask images of the i -th view. We randomly select 2 target views and set $\lambda_{lips} = 2$, $\lambda_{mask} = 0.2$ during the training stage.

4. Experiments

In this section, we evaluate PBR3DGen, detailing the experiment settings and datasets in Sec.4.1, and compare it with SOTAs in 3D generation and albedo estimation based on diffusion models across various datasets in Sec.4.2. Finally, we demonstrate the effectiveness of different components in improving PBR estimation and mesh generation in Sec. 4.3. More results are shown in the Appendix.

4.1. Experimental Setup

Dataset. We first generate multi-view PBR material training data from the Objaverse dataset [10]. Specifically, we select 48k objects by filtering out those with low-quality PBR textures, including items with black or white albedo, as well as objects missing any essential PBR attributes. For each object, we render 21-view multi-domain images (RGB, Albedo, Metallic, Roughness, Specular light) in an orbiting trajectory with uniform azimuths and varying elevations in $30^\circ, 0^\circ, -30^\circ$, under one randomly selected HDR environment map from 120 HDRI maps. The entire dataset is rendered using Blender. To evaluate the reconstruction quality of PBR materials, we randomly select 300 objects with PBR from Objaverse [10], due to the lack of publicly available PBR datasets. Additionally, we assess the quantitative performance of geometry and novel view synthesis using other public datasets, such as Google Scanned Objects (GSO) [12].

Implementation. For PBR estimation model, we use a diffusion model fine-tuned from the Stable Diffusion V2.1 [30]

based on the framework of InstructPix2Pix [3] as a starting point and continue to train for 50k iterations using an Adam [18] optimizer at a learning rate of 1×10^{-4} . For the PBR reconstruction model, we pretrain the model with only the Albedo input for 200k iterations, and then we finetune the model for 150k iterations with both Albedo and MRO image input, the MRO image encoder is initialized with the weights of the Albedo image encoder. The learning rate is 3×10^{-5} in both stages.

Metrics. We evaluate both the 2D visual quality and 3D geometric quality of the generated assets. Specifically, we assess the image quality using PSNR and MSE between the rendered and ground-truth images in both of two phases, including multi-view PBR generation and mesh generation, and we compute in the foreground region to avoid metric inflation due to the empty background. For 3D geometric evaluation, we first align the coordinate system of the generated meshes with the ground-truth meshes and report Chamfer Distance (CD) and F-Score (FS), which are computed by sampling 10K points from the surface uniformly.

4.2. Comparison with Other Methods

Baselines. We compare our results with state-of-the-art methods for both stages of our pipeline. For the multi-view PBR image generation stage, we additionally compare with IntrinsicAnything [7], a diffusion-based intrinsic image generation method. For 3D asset generation methods, we mainly focus on 3D with PBR generation models to maintain a consistent evaluation protocol across different techniques. Specifically, we compare against SF3D [2], 3DTopia-XL [8], Instantmesh [43], OpenLRM [15], LGM [38], TripoSR [40].

Results. From the 2D PBR image estimation metrics in Table 3 and Fig 5, we report our the quantitative and qualitative results outperforms IntrinsicAnything [7] on PSNR and MSE significantly.

Notably, experiments with IntrinsicAnything[7] show an abundance of black albedos, especially for metallic objects, indicating its method’s limited generalization to these materials. Nevertheless, we are able to significantly reduce the ambiguities related to these objects. Our method excels in handling highlights and shadows, particularly for metallic objects, which is essential for generating precise and reliable meshes with PBR materials in the large reconstruction module.

As shown in Table 1, Table 2, our quantitative results outperform other baselines on novel view PBR assets and geometric metrics quality across all metrics. Given that SF3D [2] and 3DTopia-XL [8] are the only recently open-sourced models capable of generating PBR assets, we compare our 2D novel view PBR materials and RGB generation results with these methods. The qualitative results for image-to-mesh and text-to-mesh generation are shown in Figs 3 and Figs 4. Our approach demonstrates superior performance



Figure 3. Qualitative comparison of the generated 3D assets with other methods.

| Methods | Albedo | | Roughness | | Metallic | | RGB | | CD↓ | Geometry | | |
|----------------|--------------|--------------|--------------|--------------|--------------|--------------|--------------|--------------|--------------|--------------|--------------|--------------|
| | PSNR↑ | MSE↓ | PSNR↑ | MSE↓ | PSNR↑ | MSE↓ | PSNR↑ | MSE↓ | | FS@0.1↑ | FS@0.2↑ | FS@0.5↑ |
| SF3D [2] | 15.98 | 0.030 | 15.00 | 0.040 | 16.04 | 0.035 | 16.37 | 0.028 | 0.332 | 0.607 | 0.787 | 0.919 |
| 3DTopia-XL [8] | 13.69 | 0.047 | 11.84 | 0.075 | 13.14 | 0.058 | 13.95 | 0.046 | 0.552 | 0.328 | 0.549 | 0.826 |
| Ours | 17.77 | 0.022 | 16.52 | 0.030 | 16.16 | 0.035 | 17.99 | 0.021 | 0.214 | 0.720 | 0.875 | 0.967 |

Table 1. Quantitative comparison on Objaverse [10] dataset.

| Methods | CD↓ | FS@0.1↑ | FS@0.2↑ | FS@0.5↑ |
|------------------|--------------|--------------|--------------|--------------|
| LGM [38] | 0.409 | 0.442 | 0.658 | 0.881 |
| OpenLRM [15] | 0.214 | 0.605 | 0.840 | 0.997 |
| TripoSR [40] | 0.356 | 0.511 | 0.727 | 0.920 |
| InstantMesh [43] | 0.216 | 0.670 | 0.862 | 0.977 |
| SF3D [2] | 0.274 | 0.554 | 0.786 | 0.956 |
| 3DTopia-XL [8] | 0.239 | 0.635 | 0.832 | 0.962 |
| Ours | 0.175 | 0.739 | 0.903 | 0.984 |

Table 2. Quantitative comparison on GSO [12] dataset.

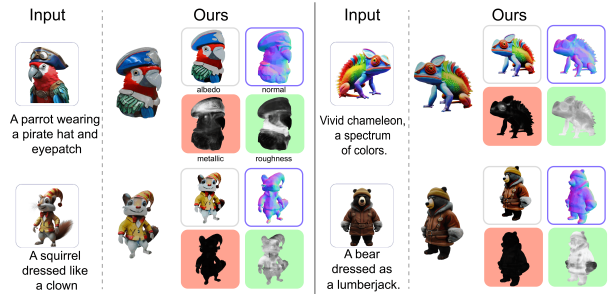


Figure 4. Text/Image to 3D results of our method.

in reconstructing shapes with detailed geometry and high-fidelity PBR textures. Thanks to the high-quality spatially-varying albedo and accurate metallic and roughness, free from any baked lighting and shadows, our relighting experiments exhibit promising results compared with other baselines. Notably, although our dataset contains fewer samples, the fine-tuning of the multi-view diffusion model with this data enables us to generate high-quality multi-view images and 3D assets with PBR.

4.3. Ablation Study

We conduct ablation studies to analyze the contribution of each component in our framework on the Objaverse PBR dataset. The key innovation of our method is its ability to effectively estimate multi-view spatially varying PBR materials. Therefore, this section focuses on evaluating the impact of the VLM-guided PBR material generation module

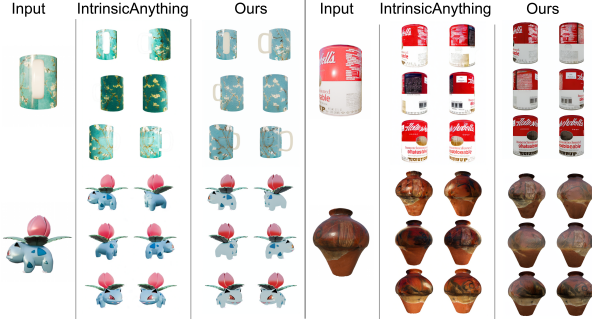


Figure 5. Qualitative comparison with IntrinsicAnything [7].

| Methods | Albedo | |
|-----------------------|-----------------|------------------|
| | PSNR \uparrow | MSE \downarrow |
| IntrinsicAnything [7] | 16.775 | 0.031 |
| Ours | 18.186 | 0.023 |
| w/o VLM-guide | 17.155 | 0.030 |

Table 3. Quantitative results for IntrinsicAnything [7] and ours. All scores are calculated as an average across 300 objects from the Objaverse dataset.

| Methods | Roughness | | Metallic | |
|-------------------------------|-----------------|------------------|-----------------|------------------|
| | PSNR \uparrow | MSE \downarrow | PSNR \uparrow | MSE \downarrow |
| w/o VD-Illum w/o VLM-guide | 18.649 | 0.020 | 15.293 | 0.0456 |
| w/o VD-Illum | 19.803 | 0.019 | 15.871 | 0.038 |
| w/o VLM-guide | 18.023 | 0.023 | 15.890 | 0.038 |
| Ours | 21.095 | 0.013 | 17.718 | 0.028 |

Table 4. Ablation studies for Multi-view PBR model. All scores are calculated as an average across 300 objects from the Objaverse dataset.

in Sec. 3.2.1 and the view-dependent illumination-aware condition module in Sec. 3.2.2. Quantitative and qualitative results are presented in Table 3, Table 4, Fig 6 and Fig 5, respectively.

(1) **w/o VD-Illum.** This term indicates training without the view-dependent illumination condition for the multi-view metallic-roughness diffusion model. As shown in Table 4 and Fig 6, VD-Illum. module as local pixel-aware priors prove to be effective for boosting the metallic-roughness distribution according to spatially varying attribution.

(2) **w/o VLM-guide.** This term indicates training without the VLM-guided condition signal for both multi-view albedo and metallic-roughness diffusion models. This is to demonstrate the necessity of introducing VLM-guided conditions for accurate PBR estimation. Table 4 clearly shows that removing the VLM-guided module leads to a remarkable decline in the performance of metallic-roughness accuracy, adversely affecting the albedo estimation as well. The qualitative results in Fig 6 further indicate the absence of VLM-guided

module results in incorrect albedo outputs with baked highlight. Simultaneously, this module plays a pivotal role in rectifying the distribution of predicted roughness and metallic values. By integrating VLM material priors for metalness and reflectivity into our metallic and roughness diffusion model, which considers materials from both global and local priors, we significantly reduce the discrepancy between predicted and actual distributions, a problem often caused by homogeneous training data.

(3) **w/o VD-Illum.& VLM-guide.** This ablation is to evaluate the multi-view PBR diffusion model without both of the above conditions. From the first column of Fig 6, it is evident that without the VLM-guided condition and the VD-illum condition, the predicted distributions for roughness and metallic are more disorganized. Additionally, the predicted values for roughness deviate significantly from the ground truth roughness image.

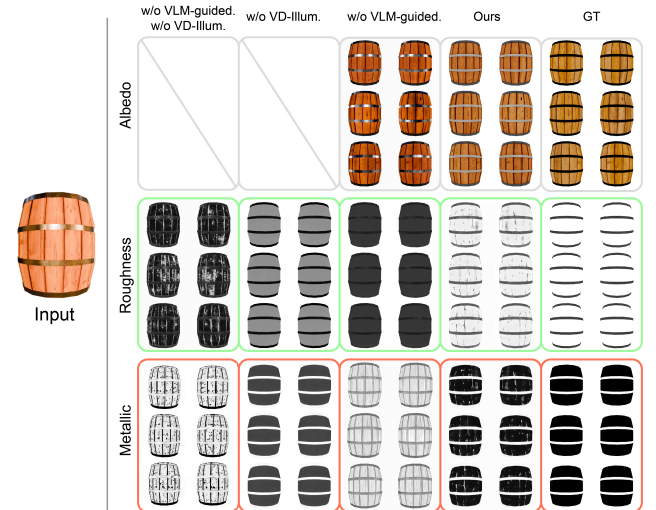


Figure 6. Qualitative ablation on PBR estimation.

4.4. Limitations and Future Work

Despite the effectiveness of our PBR3DGen, it achieves promising 3D mesh with PBR materials quality, yet it has limitations. Specifically, our framework relies on the RGB Multi-view diffusion model, which is limited by the capabilities of the Multi-View diffusion model. Poor geometric consistency can degrade the quality of our subsequent reconstruction models. In future work, we aim to improve the reconstruction of specular and transparent objects. Current diffusion models struggle to handle the geometric consistency of such objects. To address this, we plan to develop a physics-based prior that uses principles of specular reflections, refractions, and surfaces. This will enhance both the accuracy and quality of reconstructed geometry and appearance for these challenging materials.

5. Conclusion

We present PBR3DGen, a two-stage 3D mesh with high-fidelity PBR materials generation framework by introducing a novel PBR multi-view diffusion model. Specifically, we explore unleashing VLM strong material prior and view-dependent illumination-aware conditions to guide PBR multi-view generation, which significantly alleviates the ambiguity often encountered between highlights and albedo within the rendered imagery and handles spatially-varying properties. Thanks to accurate PBR multi-view images, we significantly improved 3D mesh with PBR materials reconstruction quality based on our dual-head PBR reconstruction model.

References

- [1] Sameer Agarwal, Yasutaka Furukawa, Noah Snavely, Ian Simon, Brian Curless, Steven M Seitz, and Richard Szeliski. Building rome in a day. *Communications of the ACM*, 54(10): 105–112, 2011. 3
- [2] Mark Boss, Zixuan Huang, Aaryaman Vasishta, and Varun Jampani. Sf3d: Stable fast 3d mesh reconstruction with uv-unwrapping and illumination disentanglement. *arXiv preprint arXiv:2408.00653*, 2024. 2, 5, 6, 7
- [3] Tim Brooks, Aleksander Holynski, and Alexei A Efros. Instructpix2pix: Learning to follow image editing instructions. In *Proceedings of the IEEE/CVF Conference on Computer Vision and Pattern Recognition*, 2023. 6
- [4] Tianshi Cao, Karsten Kreis, Sanja Fidler, Nicholas Sharp, and Kangxue Yin. Textfusion: Synthesizing 3d textures with text-guided image diffusion models. In *Proceedings of the IEEE/CVF International Conference on Computer Vision*, 2023. 3
- [5] Dave Zhenyu Chen, Yawar Siddiqui, Hsin-Ying Lee, Sergey Tulyakov, and Matthias Nießner. Text2tex: Text-driven texture synthesis via diffusion models. In *Proceedings of the IEEE/CVF International Conference on Computer Vision*, 2023. 3
- [6] Rui Chen, Yongwei Chen, Ningxin Jiao, and Kui Jia. Fantasia3d: Disentangling geometry and appearance for high-quality text-to-3d content creation. In *Proceedings of the IEEE/CVF international conference on computer vision*, 2023. 3
- [7] Xi Chen, Sida Peng, Dongchen Yang, Yuan Liu, Bowen Pan, Chengfei Lv, and Xiaowei Zhou. Intrinsicanything: Learning diffusion priors for inverse rendering under unknown illumination. *arXiv preprint arXiv:2404.11593*, 2024. 3, 4, 6, 8
- [8] Zhaoxi Chen, Jiaxiang Tang, Yuhao Dong, Ziang Cao, Fangzhou Hong, Yushi Lan, Tengfei Wang, Haozhe Xie, Tong Wu, Shunsuke Saito, et al. 3dtopia-xl: Scaling high-quality 3d asset generation via primitive diffusion. *arXiv preprint arXiv:2409.12957*, 2024. 2, 6, 7
- [9] Robert L Cook and Kenneth E. Torrance. A reflectance model for computer graphics. *ACM Transactions on Graphics (ToG)*, 1(1), 1982. 5, 1
- [10] Matt Deitke, Dustin Schwenk, Jordi Salvador, Luca Weihs, Oscar Michel, Eli VanderBilt, Ludwig Schmidt, Kiana Ehsani, Aniruddha Kembhavi, and Ali Farhadi. Objaverse: A universe of annotated 3d objects. In *Proceedings of the IEEE/CVF Conference on Computer Vision and Pattern Recognition*, 2023. 2, 5, 6, 7
- [11] Kangle Deng, Timothy Omerick, Alexander Weiss, Deva Ramanan, Jun-Yan Zhu, Tinghui Zhou, and Maneesh Agrawala. Flashtex: Fast relightable mesh texturing with lightcontrolnet. *arXiv preprint arXiv:2402.13251*, 2024. 3
- [12] Laura Downs, Anthony Francis, Nate Koenig, Brandon Kinman, Ryan Hickman, Krista Reymann, Thomas B McHugh, and Vincent Vanhoucke. Google scanned objects: A high-quality dataset of 3d scanned household items. In *2022 International Conference on Robotics and Automation (ICRA)*. IEEE, 2022. 6, 7
- [13] Ye Fang, Zeyi Sun, Tong Wu, Jiaqi Wang, Ziwei Liu, Gordon Wetzstein, and Dahua Lin. Make-it-real: Unleashing large multimodal model for painting 3d objects with realistic materials. *arXiv preprint arXiv:2404.16829*, 3, 2024. 5
- [14] Yasutaka Furukawa and Jean Ponce. Accurate, dense, and robust multiview stereopsis. *IEEE transactions on pattern analysis and machine intelligence*, 32(8):1362–1376, 2009. 3
- [15] Zexin He and Tengfei Wang. Openlrm: Open-source large reconstruction models, 2023. 6, 7
- [16] Yicong Hong, Kai Zhang, Jiuxiang Gu, Sai Bi, Yang Zhou, Difan Liu, Feng Liu, Kalyan Sunkavalli, Trung Bui, and Hao Tan. Lrm: Large reconstruction model for single image to 3d. *arXiv preprint arXiv:2311.04400*, 2023. 3
- [17] Bernhard Kerbl, Georgios Kopanas, Thomas Leimkühler, and George Drettakis. 3d gaussian splatting for real-time radiance field rendering. *ACM Trans. Graph.*, 42(4):139–1, 2023. 5
- [18] Diederik P Kingma. Adam: A method for stochastic optimization. *arXiv preprint arXiv:1412.6980*, 2014. 6
- [19] Peng Li, Yuan Liu, Xiaoxiao Long, Feihu Zhang, Cheng Lin, Mengfei Li, Xingqun Qi, Shanghang Zhang, Wenhan Luo, Ping Tan, et al. Era3d: High-resolution multiview diffusion using efficient row-wise attention. *arXiv preprint arXiv:2405.11616*, 2024. 3
- [20] Sixu Li, Chaojian Li, Wenbo Zhu, Boyang Yu, Yang Zhao, Cheng Wan, Haoran You, Huihong Shi, and Yingyan Lin. Instant-3d: Instant neural radiance field training towards on-device ar/vr 3d reconstruction. In *Proceedings of the 50th Annual International Symposium on Computer Architecture*, pages 1–13, 2023. 3
- [21] Yuan Li, Xiangyang He, Yankai Jiang, Huan Liu, Yubo Tao, and Lin Hai. Meshformer: High-resolution mesh segmentation with graph transformer. In *Computer Graphics Forum*, pages 37–49. Wiley Online Library, 2022. 3
- [22] Yuan Liu, Cheng Lin, Zijiao Zeng, Xiaoxiao Long, Lingjie Liu, Taku Komura, and Wenping Wang. Syncdreamer: Generating multiview-consistent images from a single-view image. *arXiv preprint arXiv:2309.03453*, 2023. 3
- [23] Yuxin Liu, Minshan Xie, Hanyuan Liu, and Tien-Tsin Wong. Text-guided texturing by synchronized multi-view diffusion. *arXiv preprint arXiv:2311.12891*, 2023. 3
- [24] Xiaoxiao Long, Yuan-Chen Guo, Cheng Lin, Yuan Liu, Zhiyang Dou, Lingjie Liu, Yuexin Ma, Song-Hai Zhang, Marc Habermann, Christian Theobalt, et al. Wonder3d: Single image to 3d using cross-domain diffusion. In *Proceedings of*

- the *IEEE/CVF Conference on Computer Vision and Pattern Recognition*, pages 9970–9980, 2024. 2, 3
- [25] Ben Mildenhall, Pratul P Srinivasan, Matthew Tancik, Jonathan T Barron, Ravi Ramamoorthi, and Ren Ng. Nerf: Representing scenes as neural radiance fields for view synthesis. *Communications of the ACM*, 65(1):99–106, 2021. 5
- [26] Marc Pollefeys, Luc Van Gool, Maarten Vergauwen, Frank Verbiest, Kurt Cornelis, Jan Tops, and Reinhard Koch. Visual modeling with a hand-held camera. *International Journal of Computer Vision*, 59:207–232, 2004. 3
- [27] Marc Pollefeys, David Nistér, J-M Frahm, Amir Akbarzadeh, Philippos Mordohai, Brian Clipp, Chris Engels, David Gallup, S-J Kim, Paul Merrell, et al. Detailed real-time urban 3d reconstruction from video. *International Journal of Computer Vision*, 78:143–167, 2008. 3
- [28] Alec Radford, Jong Wook Kim, Chris Hallacy, Aditya Ramesh, Gabriel Goh, Sandhini Agarwal, Girish Sastry, Amanda Askell, Pamela Mishkin, Jack Clark, et al. Learning transferable visual models from natural language supervision. In *International conference on machine learning*. PMLR, 2021. 5, 2
- [29] Elad Richardson, Gal Metzer, Yuval Alaluf, Raja Giryes, and Daniel Cohen-Or. Texture: Text-guided texturing of 3d shapes. In *ACM SIGGRAPH 2023 conference proceedings*, 2023. 3
- [30] Robin Rombach, Andreas Blattmann, Dominik Lorenz, Patrick Esser, and Björn Ommer. High-resolution image synthesis with latent diffusion models. In *Proceedings of the IEEE/CVF conference on computer vision and pattern recognition*, 2022. 6
- [31] Johannes L Schonberger and Jan-Michael Frahm. Structure-from-motion revisited. In *Proceedings of the IEEE conference on computer vision and pattern recognition*, pages 4104–4113, 2016. 3
- [32] Johannes L Schönberger, Enliang Zheng, Jan-Michael Frahm, and Marc Pollefeys. Pixelwise view selection for unstructured multi-view stereo. In *Computer Vision–ECCV 2016: 14th European Conference, Amsterdam, The Netherlands, October 11–14, 2016, Proceedings, Part III 14*, pages 501–518. Springer, 2016. 3
- [33] Tianchang Shen, Jun Gao, Kangxue Yin, Ming-Yu Liu, and Sanja Fidler. Deep marching tetrahedra: a hybrid representation for high-resolution 3d shape synthesis. *Advances in Neural Information Processing Systems*, 34:6087–6101, 2021. 5
- [34] Tianchang Shen, Jacob Munkberg, Jon Hasselgren, Kangxue Yin, Zian Wang, Wenzheng Chen, Zan Gojcic, Sanja Fidler, Nicholas Sharp, and Jun Gao. Flexible isosurface extraction for gradient-based mesh optimization. *ACM Trans. Graph.*, 42(4):37–1, 2023. 5
- [35] Ruoxi Shi, Hansheng Chen, Zhuoyang Zhang, Minghua Liu, Chao Xu, Xinyue Wei, Linghao Chen, Chong Zeng, and Hao Su. Zero123++: a single image to consistent multi-view diffusion base model. *arXiv preprint arXiv:2310.15110*, 2023. 2, 3, 4
- [36] Yichun Shi, Peng Wang, Jianglong Ye, Mai Long, Kejie Li, and Xiao Yang. Mvdream: Multi-view diffusion for 3d generation. *arXiv preprint arXiv:2308.16512*, 2023. 3
- [37] Yawar Siddiqui, Tom Monnier, Filippos Kokkinos, Mahendra Kariya, Yanir Kleiman, Emilien Garreau, Oran Gafni, Natalia Neverova, Andrea Vedaldi, Roman Shapovalov, et al. Meta 3d assetgen: Text-to-mesh generation with high-quality geometry, texture, and pbr materials. *arXiv preprint arXiv:2407.02445*, 2024. 2, 5
- [38] Jiayang Tang, Zhaoxi Chen, Xiaokang Chen, Tengfei Wang, Gang Zeng, and Ziwei Liu. Lgm: Large multi-view gaussian model for high-resolution 3d content creation. In *European Conference on Computer Vision*. Springer, 2025. 6, 7
- [39] Shitao Tang, Fuyang Zhang, Jiacheng Chen, Peng Wang, and Yasutaka Furukawa. Mvdiffrusion: Enabling holistic multi-view image generation with correspondence-aware diffusion. *arXiv*, 2023. 2, 3
- [40] Dmitry Tochilkin, David Pankratz, Zexiang Liu, Zixuan Huang, Adam Letts, Yangguang Li, Ding Liang, Christian Laforte, Varun Jampani, and Yan-Pei Cao. Triposr: Fast 3d object reconstruction from a single image. *arXiv preprint arXiv:2403.02151*, 2024. 6, 7
- [41] Peng Wang, Lingjie Liu, Yuan Liu, Christian Theobalt, Taku Komura, and Wenping Wang. Neus: Learning neural implicit surfaces by volume rendering for multi-view reconstruction. *arXiv preprint arXiv:2106.10689*, 2021. 5
- [42] Xinyue Wei, Kai Zhang, Sai Bi, Hao Tan, Fujun Luan, Valentin Deschaintre, Kalyan Sunkavalli, Hao Su, and Zexiang Xu. Meshlrn: Large reconstruction model for high-quality mesh. *arXiv preprint arXiv:2404.12385*, 2024. 3
- [43] Jiale Xu, Weihao Cheng, Yiming Gao, Xintao Wang, Shenghua Gao, and Ying Shan. Instantmesh: Efficient 3d mesh generation from a single image with sparse-view large reconstruction models. *arXiv preprint arXiv:2404.07191*, 2024. 2, 3, 6, 7
- [44] Xianghui Yang, Huiwen Shi, Bowen Zhang, Fan Yang, Jiacheng Wang, Hongxu Zhao, Xinhai Liu, Xinzhou Wang, Qingxiang Lin, Jiao Yu, et al. Hunyuan3d-1.0: A unified framework for text-to-3d and image-to-3d generation. *arXiv preprint arXiv:2411.02293*, 2024. 5
- [45] Xianfang Zeng, Xin Chen, Zhongqi Qi, Wen Liu, Zibo Zhao, Zhibin Wang, Bin Fu, Yong Liu, and Gang Yu. Paint3d: Paint anything 3d with lighting-less texture diffusion models. In *Proceedings of the IEEE/CVF Conference on Computer Vision and Pattern Recognition*, pages 4252–4262, 2024. 3
- [46] Zheng Zeng, Valentin Deschaintre, Iliyan Georgiev, Yannick Hold-Geoffroy, Yiwei Hu, Fujun Luan, Ling-Qi Yan, and Miloš Hašan. Rgb \leftrightarrow x: Image decomposition and synthesis using material-and lighting-aware diffusion models. In *ACM SIGGRAPH 2024 Conference Papers*, 2024. 3, 4
- [47] Chubin Zhang, Hongliang Song, Yi Wei, Yu Chen, Jiwen Lu, and Yansong Tang. Geolrm: Geometry-aware large reconstruction model for high-quality 3d gaussian generation. *arXiv preprint arXiv:2406.15333*, 2024. 3
- [48] Kai Zhang, Sai Bi, Hao Tan, Yuanbo Xiangli, Nanxuan Zhao, Kalyan Sunkavalli, and Zexiang Xu. Gs-lrm: Large reconstruction model for 3d gaussian splatting. In *European Conference on Computer Vision*, pages 1–19. Springer, 2025. 3

- [49] Longwen Zhang, Ziyu Wang, Qixuan Zhang, Qiwei Qiu, Anqi Pang, Haoran Jiang, Wei Yang, Lan Xu, and Jingyi Yu. Clay: A controllable large-scale generative model for creating high-quality 3d assets. *ACM Transactions on Graphics (TOG)*, 43(4):1–20, 2024. [2](#), [5](#)

PBR3DGen: A VLM-guided Mesh Generation with High-quality PBR Texture

Supplementary Material

6. Details of Methods

6.1. Physically-based Rendering Model

The traditional rendering equation [?] is formulated following the principles of energy conservation in physics. It computes the outgoing radiance L_o at surface point $\hat{\mathbf{x}}$ with surface normal $\hat{\mathbf{n}}_x$ along view direction ω_o by integrating over the hemisphere $\Omega^+ = \{\omega_i : \omega_i \cdot \hat{\mathbf{n}}_x > 0\}$, where ω_i is the incident light direction:

$$L_o(\hat{\mathbf{x}}, \omega_o) = \int_{\Omega^+} L_i(\hat{\mathbf{x}}, \omega_i) f_r(\hat{\mathbf{x}}, \omega_i, \omega_o) (\omega_i \cdot \hat{\mathbf{n}}_x) d\omega_i \quad (7)$$

The function $L_i(\hat{\mathbf{x}}, \omega_i)$ represents the incoming radiance at the surface point $\hat{\mathbf{x}}$ from ω_i , while the BRDF function f_r quantifies the proportion of light arriving from direction ω_i that is reflected in the direction ω_o at point $\hat{\mathbf{x}}$.

In Sec.3.2, We propose a **view-dependent illumination-aware condition** based on the microfacet BRDF model [?] to approximate surface reflectance properties using a set of decomposed intrinsic terms, such as Roughness and Metallic, which encapsulate the interaction of light with a surface. The microfacet model provides a robust framework for simulating the reflection from rough surfaces. The BRDF $f_r(\hat{\mathbf{x}}, \omega_i, \omega_o)$ is the ratio between the incoming and outgoing radiance. It is a function of the surface location $\hat{\mathbf{x}}$, incoming direction ω_i , and the outgoing direction ω_o :

$$f_r(\hat{\mathbf{x}}, \omega_i, \omega_o) = f_d(\hat{\mathbf{x}}) + f_s(\hat{\mathbf{x}}, \omega_i, \omega_o) \quad (8)$$

where the BRDF comprises diffuse reflection f_d and specular reflection f_s . In the first stage of BRDF estimation, we use the diffuse reflection term $f_d(\hat{\mathbf{x}}) = \frac{\hat{\mathbf{A}}_x}{\pi}$ based on a simple Lambertian model. Here, we introduce the specular BRDF f_s which follows the Cook-Torrance model [9]:

$$f_s = \frac{D(\mathbf{h}, \hat{\mathbf{n}}, R) \cdot F(\omega_o, \mathbf{h}) \cdot G(\omega_i, \omega_o, \hat{\mathbf{n}}, R)}{4(\hat{\mathbf{n}} \cdot \omega_o)(\hat{\mathbf{n}} \cdot \omega_i)} \quad (9)$$

where $\hat{\mathbf{n}}$ is the surface normal at $\hat{\mathbf{x}}$, R is roughness term, \mathbf{h} is a half vector, D denotes Normal Distribution Function (NDF), F denotes Fresnel function and G is the Geometry Factor.

The normal distribution function D describes the probability density of microfacet orientations aligned with the half-vector \mathbf{h} . It is dependent on the macroscopic normal \mathbf{h} and the surface roughness R , influencing the distribution of specular highlights, as follows:

$$D(\mathbf{h}, \hat{\mathbf{n}}, R) = \frac{R^2}{\pi((\hat{\mathbf{n}} \cdot \mathbf{h})^2(R^2 - 1) + 1)^2} \quad (10)$$

where the half-vector \mathbf{h} is the normalized vector halfway between the incident light direction and the reflection direction, $\hat{\mathbf{n}}$ is the macroscopic surface normal, and $R = R^2$ is the surface roughness parameter, ranging from [0,1]. As R approaches 0, the surface tends towards a mirror-like reflection, while R approaching 1 indicates an extremely rough surface.

In the microfacet BRDF model, the Fresnel reflectance term F characterizes the proportion of light reflected from a material's surface at varying angles of incidence. This proportion changes with the angle of incidence, being lowest at normal incidence and highest at grazing angles for non-metallic materials. The Fresnel term can be efficiently computed using Schlick's approximation [?]:

$$F(\omega_o, \mathbf{h}) = F_0 + (1 - F_0) \cdot (1 - (\omega_o \cdot \mathbf{h}))^5 \quad (11)$$

where F_0 is the reflectance at normal incidence, also known as the base reflectance and $\omega_o \cdot \mathbf{h}$ is the dot product between the outgoing radiance and the half-vector, dictating the cosine of the angle of incidence. F_0 is up to the intrinsic properties of the material, typically categorized as insulators or metals, and higher metallic leads to a higher F_0 .

In the realm of Physically Based Rendering (PBR), particularly within the context of the GGX Specular reflection model, the Geometry Function G assumes a pivotal role. It is primarily responsible for simulating the occlusion and shadowing effects attributable to the microsurface structure, crucial for accurately rendering light reflections on rough surfaces. The geometry function is typically computed using a combination of the Smith geometry function and the Schlick-GGX approximation. This formula is written as:

$$G(\hat{\mathbf{n}}, \omega_o, \omega_i, R) = G_1(\hat{\mathbf{n}}, \omega_o, R) \cdot G_1(\hat{\mathbf{n}}, \omega_i, R) \quad (12)$$

Here, G_1 represents the monodirectional shadowing function:

$$G_1(\hat{\mathbf{n}}, \omega_o, R) = \frac{\hat{\mathbf{n}} \cdot \omega_o}{(\hat{\mathbf{n}} \cdot \omega_o)(1 - k) + k} \quad (13)$$

$$G_1(\hat{\mathbf{n}}, \omega_i, R) = \frac{\hat{\mathbf{n}} \cdot \omega_i}{(\hat{\mathbf{n}} \cdot \omega_i)(1 - k) + k} \quad (14)$$

where R is the parameter indicating surface roughness, k is a parameter derived from the roughness, typically calculated as $k = \frac{R^2}{2}$.

6.2. VLM-guided PBR Material generation

For alleviating these hard ambiguities between Albedo and specular light derived from Albedo generation and due to Roughness and Metallic distribution for objects tend to be

part-aware consistent, we leverage VLM to provide strong prior to alleviate these hard ambiguities. Specifically, we design the a two-round reflective-metalness material dialogue mechanism (RMD) by GPT-4V, which can effectively unleash the ability for reflective material knowledge. We observe that VLM not only accurately identifies whether materials are metallic or reflective but also determines material properties at the component level, as shown in the Fig. 17. Using the CLIP [28] model allows us to integrate this prior knowledge into the material generation process.

7. Additional Results of Experiments

7.1. Mutil-view PBR Comparison results

We show more results on text-to-mesh task compared with other baselines, see in Fig. 7 and Fig. 8.

7.2. Text-to-mesh Comparison results

As shown in Fig. 9, we also implement our method on text-to-mesh task compared with other baselines. The images are generated by HunyuanDiT[?] conditioned on text prompts, and we remove their background.

7.3. Image-to-mesh Comparison results

We show more results on text-to-mesh task compared with other baselines, see in Fig. 10 and Fig. 11.

7.4. Abaltion results for Multi-view PBR estimation

We show more results on abaltion study results for Albedo and MRO maps, see in Fig. 15 and Fig. 18.

7.5. Comparison results for PBR estimation

Given the lack of large-scale PBR datasets and the difficulty in obtaining real-world PBR, we used the only publicly available PBR dataset from Objaverse for intrinsic image evaluation. Additionally, we evaluated our RGB and geometry metric on the GSO dataset, outperforming existing methods. To further validate our results, we add FID metrics on both Objaverse and GSO datasets in Table. 6.

7.6. Robust experiments for PBR estimation:

We add the distribution of predicted albedo in Fig. 12(a). Our outperforms IntrinsicAnything with 8.4% higher PSNR and 25.5% lower MSE, alongside **5.7%** and **30.9%** reductions in **Standard Deviation**, respectively, demonstrating superior robustness and accuracy.

Meanwhile, we test our PBR diffsuion model on two real-world dataset, GSO and MVImgNet. Our method outperforms IntrinsicAnything, especially on reflective surfaces, reducing lighting and shadow ambiguity in Fig. 13.

7.7. Method of feature injection:

Our injects features via latent noise concatenation, outperforming IP-Adapter and ControlNet in pixel-level alignment of image contours and structures, as shown in Table. 5.

Table 5. Comparison of different injection methods.

| Methods | Albedo | | Metallic | | Roughness | |
|---------------------|---------------|--------------|---------------|--------------|---------------|--------------|
| | PSNR | MSE | PSNR | MSE | PSNR | MSE |
| ControlNet | 17.874 | 0.025 | 16.451 | 0.039 | 16.960 | 0.031 |
| Ip-adapter | 17.351 | 0.029 | 16.546 | 0.038 | 15.932 | 0.036 |
| Concat(Ours) | 18.186 | 0.023 | 17.718 | 0.028 | 21.095 | 0.013 |
| Five-channel | 16.986 | 0.033 | 17.118 | 0.031 | 20.985 | 0.016 |

In PBR rendering, metallic/roughness control reflective effects while albedo defines base color. These material properties are independent: an object may share metallic values but differ in color. Using separate latent spaces aligns with physical rendering principles. Additionally, specular light condition affects only metallic/roughness, and independent encoding avoids interference with albedo sampling. The results in Table. 5 further validate our idea.

7.8. Specular illumination maps:

We directly rendered the specular light map using Blender as GT. As shown in Fig. 14, the distinct highlights on the chair back and leather regions in the specular light map guide spatially varying roughness generation and further improve roughness/metallic accuracy.

8. Applications

Based on our PBR model, we can further relight and animate the model under different illumination, as shown in Fig. 16. More video results and visualization can be found on our project page: <https://pbr3dgen1218.github.io/>.

Table 6. FID(↓) comparison on GSO and Objaverse.

| Methods | Ours | SF3D | PrimX | OpenLRM | TripoSr | InstantMesh | LGM |
|-------------------|--------------|-------|-------|---------|---------|-------------|--------|
| RGB(GSO) | 65.04 | 87.32 | 75.86 | 113.42 | 109.32 | 91.32 | 132.64 |
| RGB(Objaverse) | 49.37 | 55.36 | 68.49 | - | - | - | - |
| Albedo(Objaverse) | 50.63 | 57.67 | 78.55 | - | - | - | - |



Figure 7. Qualitative comparison with IntrinsicAnything [7] on multi-view PBR estimation.

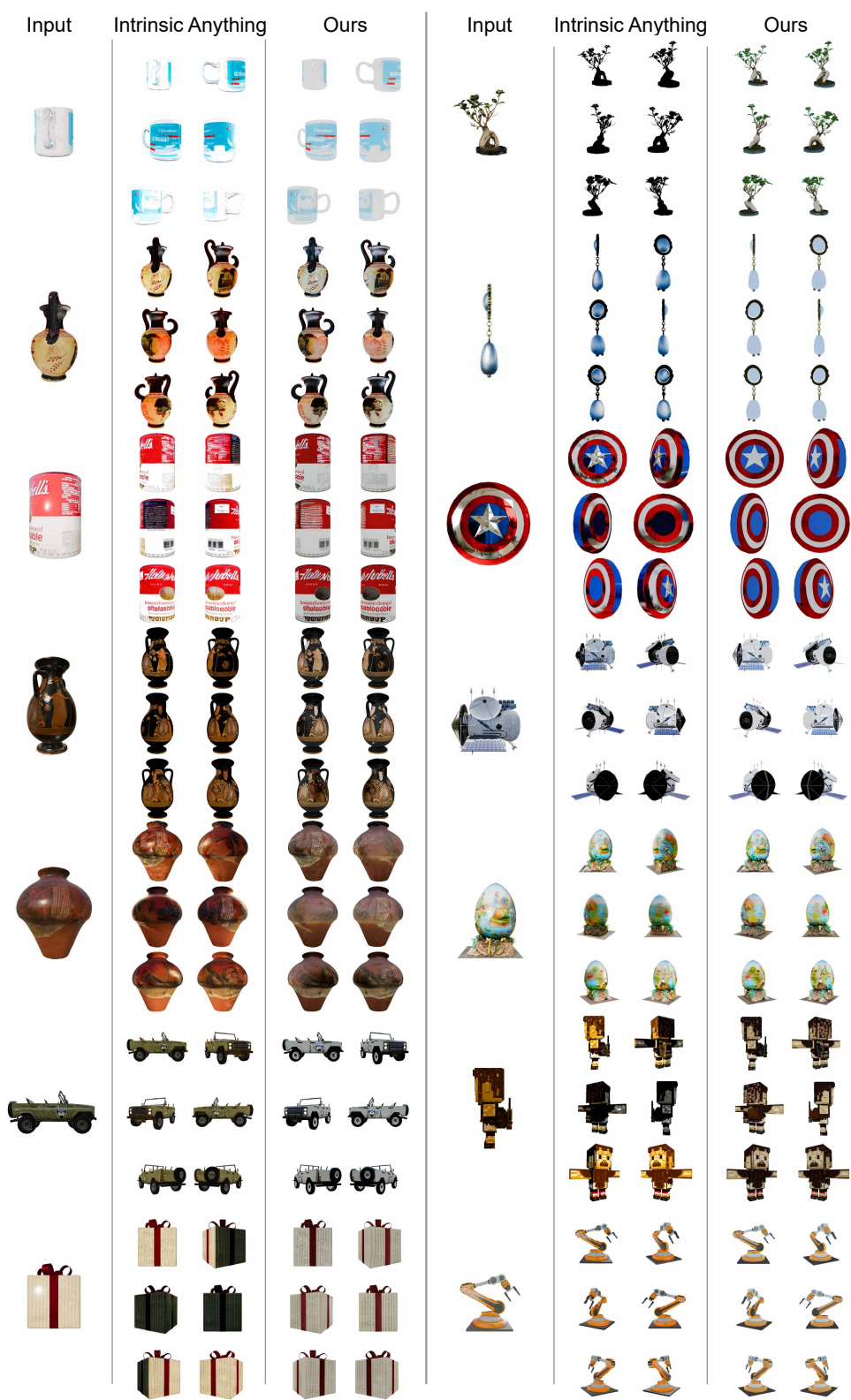


Figure 8. Qualitative comparison with IntrinsicAnything [7] on multi-view PBR estimation.

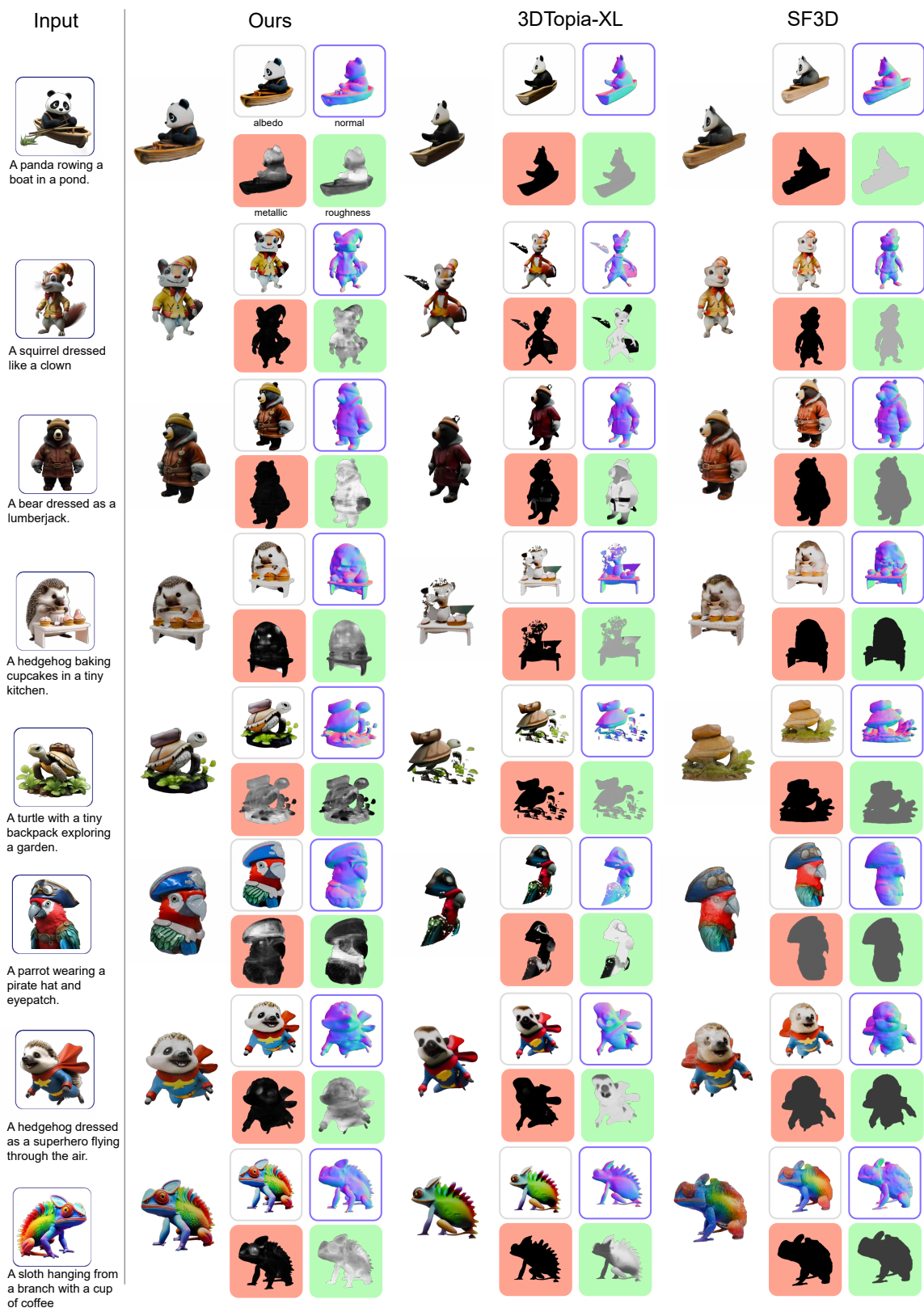


Figure 9. Qualitative comparison of the generated 3D assets with other methods on Text-to-mesh.

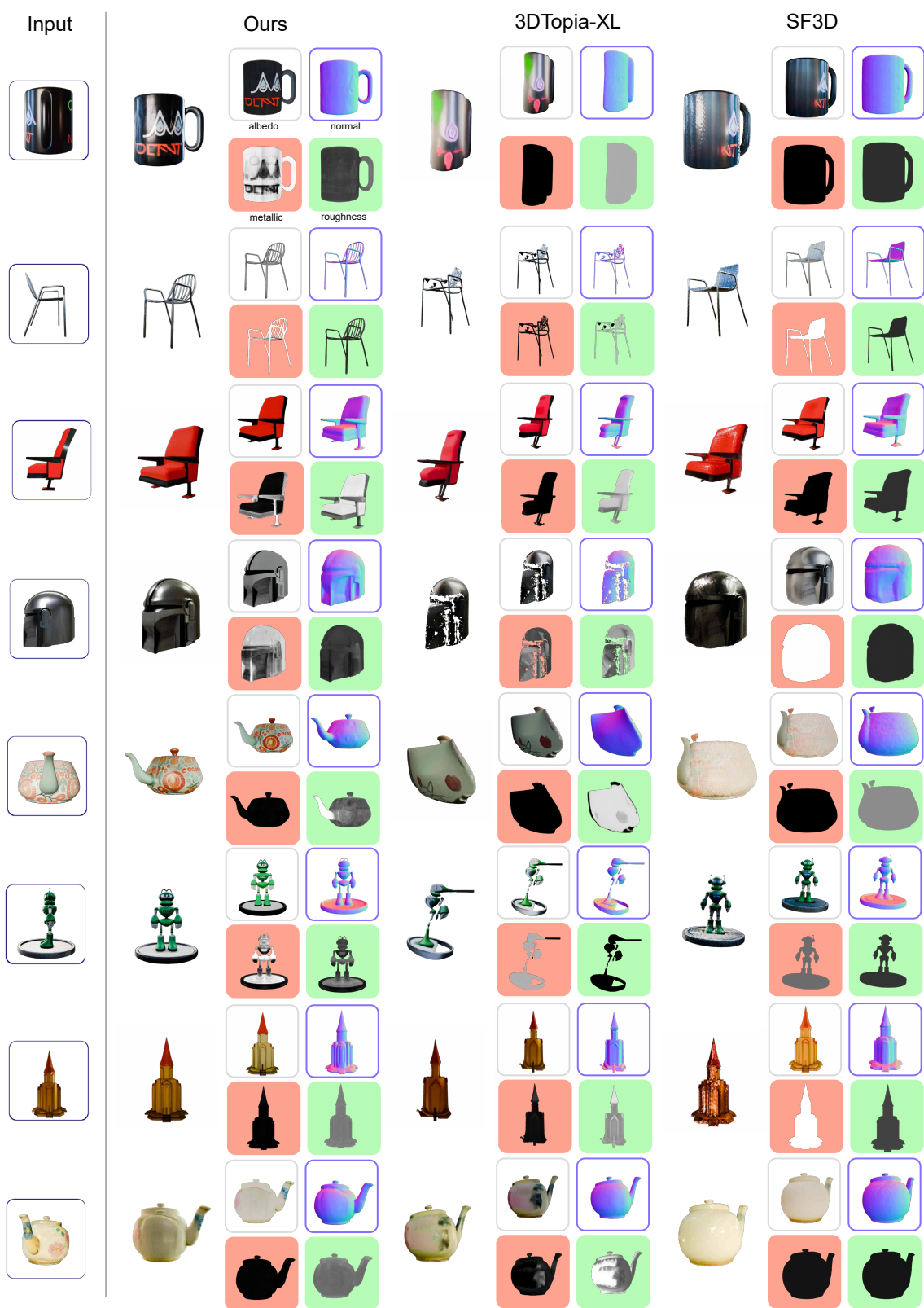


Figure 10. Qualitative comparison of the generated 3D assets with other methods on Image-to-mesh.



Figure 11. Qualitative comparison of the generated 3D assets with other methods on Image-to-mesh.

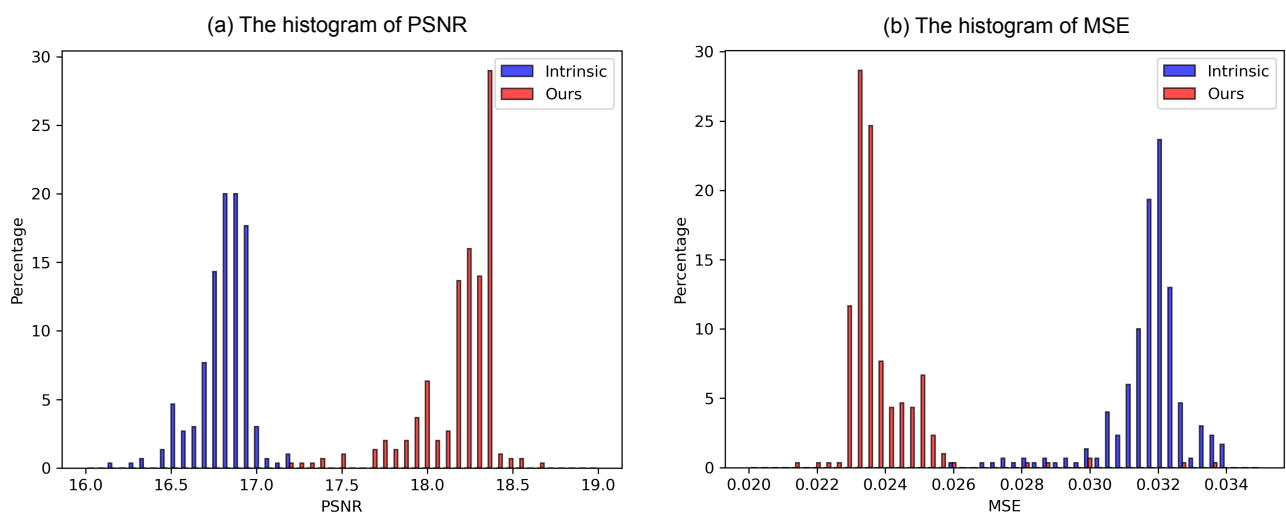


Figure 12. Quantitative results on PBR estimation robust experiments.

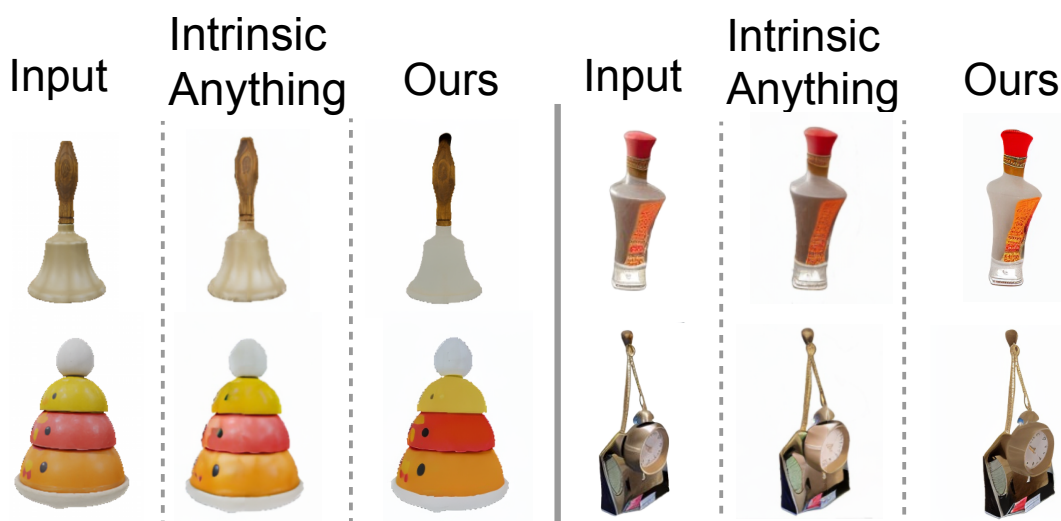


Figure 13. Qualitative PBR results on real-world data.

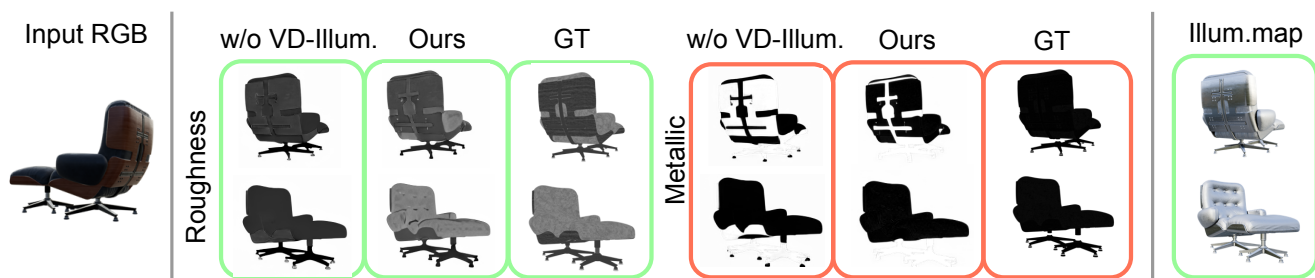


Figure 14. The qualitative result for specular light condition.

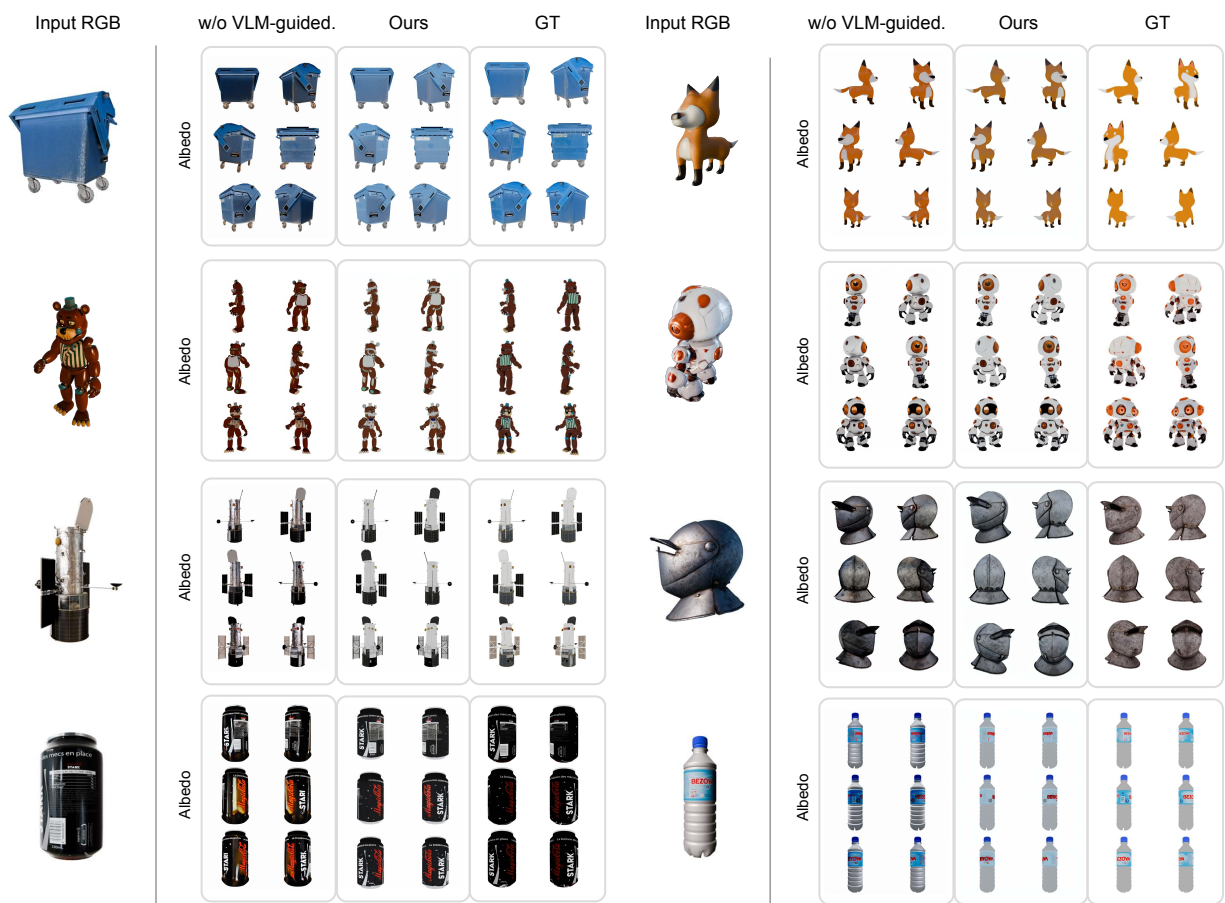


Figure 15. Ablation studies for Multiview albedo estimation. All scores are calculated as an average across 300 objects from the Objaverse dataset.

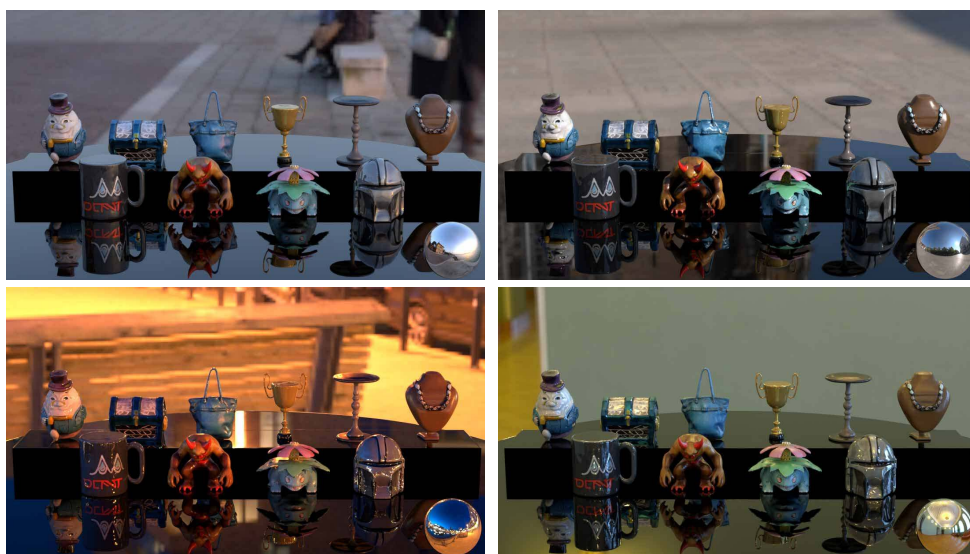


Figure 16. Relighting results under different environment illumination.

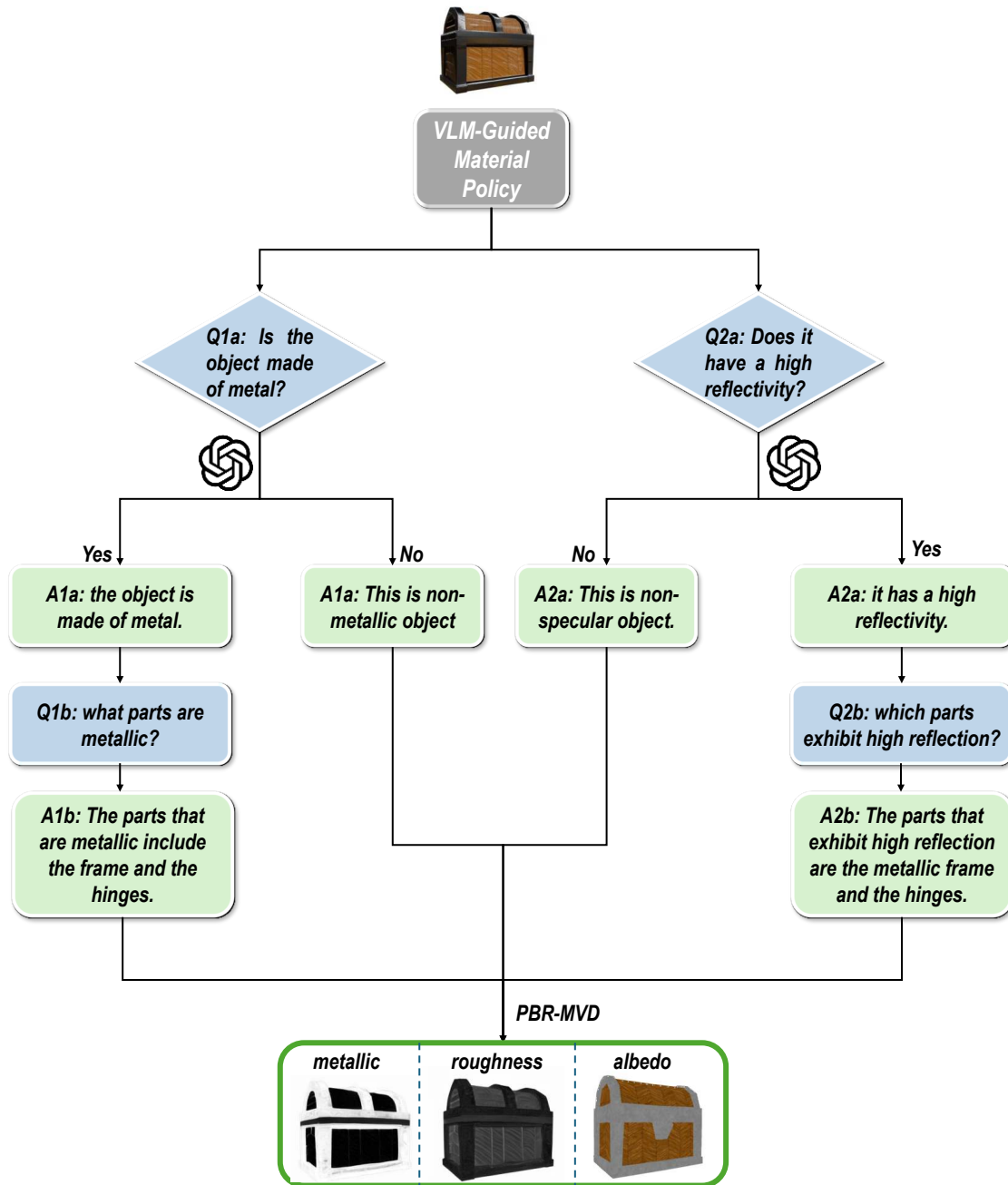


Figure 17. The VLM-Guided material policy, including two-round reflective-metalness material dialogue mechanism.

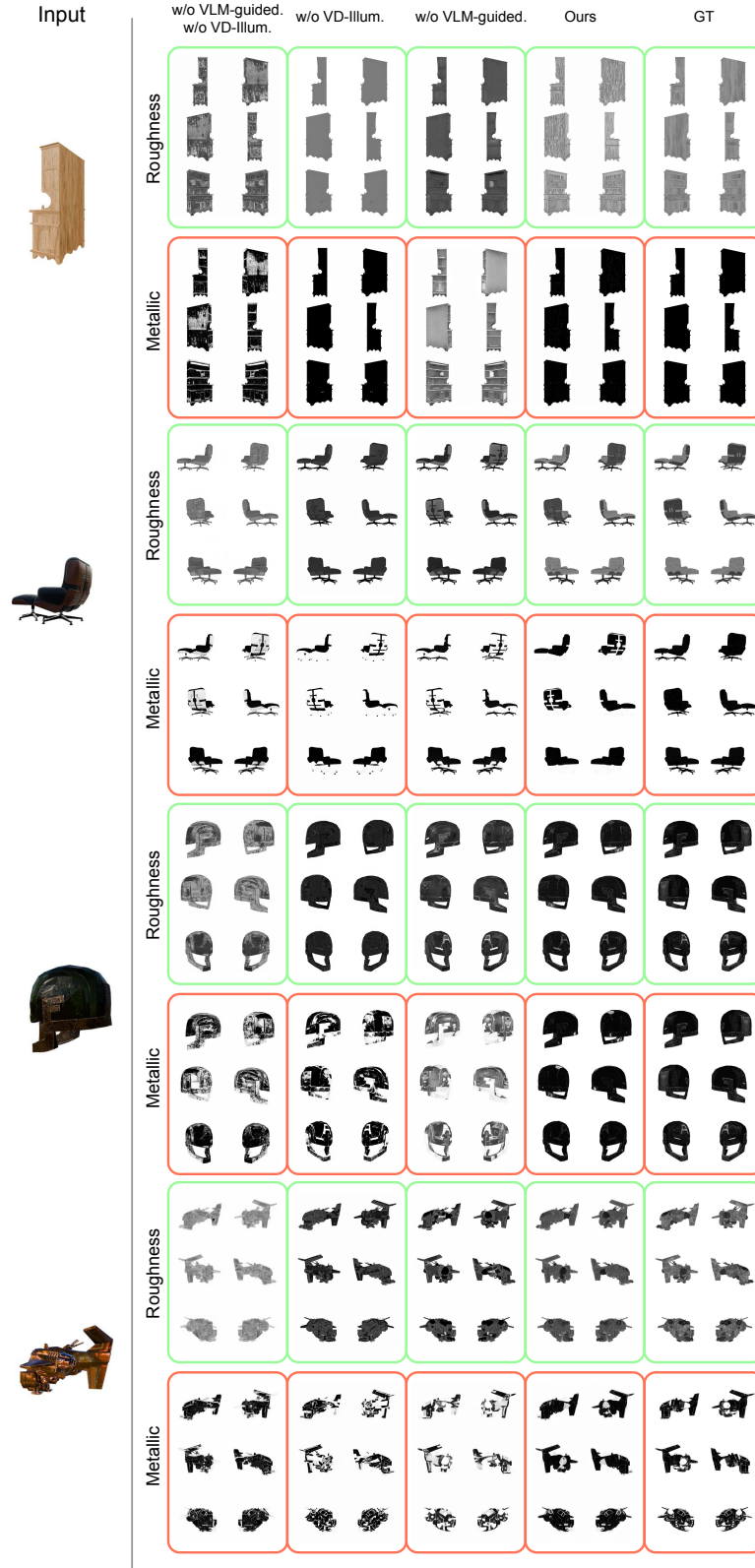


Figure 18. Ablation studies for Multiview metallic and roughness estimation. All scores are calculated as an average across 300 objects from the Objaverse dataset.